ACS EARTH AND SPACE CHEMISTRY

http://pubs.acs.org/journal/aesccq

Article

Simulating the Impact of Long-Range-Transported Asian Mineral Dust on the Formation of Sulfate and Nitrate during the KORUS-AQ Campaign

Zechen Yu, Myoseon Jang,* Soontae Kim, Changhan Bae, Bonyoung Koo, Ross Beardsley, Jinsoo Park, Lim Seok Chang, Hee Choon Lee, Yun-Kyu Lim, and Jeong Hoon Cho

Cite This: https://dx.doi.org/10.1021/acsearthspacechem.0c00074

Read Online

ACCESS | Metrics & More | Article Recommendations | Supporting Information

ABSTRACT: The atmospheric mineral aerosol reaction (AMAR) model, which was developed to simulate dust-driven heterogeneous chemistry of SO_2 and NO_x, was combined with the comprehensive air quality model with extensions (CAMx). The resulting model was then applied to simulate the influence of the long-range-transported dust particles on the formation of sulfate and nitrate during the Korean-United States Air Quality (KORUS-AQ) campaign from May 19 to 30, 2016. In the mechanisms, dust particles promoted the oxidation of SO_2 and NO_x through heterogeneous photocatalytic reactions and autoxidation. The predicted concentrations of sulfate, nitrate, and ammonium ions were compared with ground-based observations obtained at a monitoring site in Olympic Park, Seoul, Korea. The predicted sulfate increased by 29% in the high dust period of this campaign, while the sulfate produced via nondust aqueous reactions decreased by 66%. The model captured the impact of dust on the sulfate formation in that particulate sulfate increased with increasing dust loads. The model also predicted the formation of a large quantity of particulate nitrate during the cold and wet periods in the presence of abundant ammonia in East Asia. The trajectory simulations showed that dust particles were rapidly buffered by sulfate when dust parcels passed urban and industrial areas in Asia and then heavily coated with sulfate and nitrate during long-range transport. The KORUS-AQ campaign was conducted after passing the dust season (i.e., springtime), although dust concentrations were still higher than those in ordinary seasons. Thus, the impact of dust particles on the formation of sulfate and nitrate will be more significant during dust events.

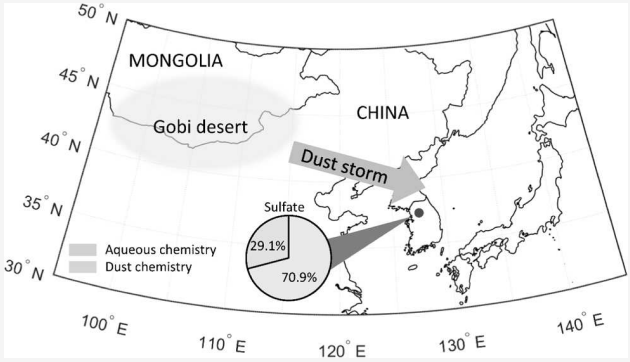

KEYWORDS: *KORUS-AQ, mineral dust, sulfate, nitrate, CAMx, heterogeneous chemistry*

■ INTRODUCTION

Airborne dust particles, originating from desert and semidesert regions, can transport across continents during seasonal wind episodes. The annual global emissions of airborne mineral dust particles are estimated to be between 1000 and 3000 Tg.[1,2] This long-range transport of dust particles is influenced by their particle size distribution. For example, coarse dust particles are deposited locally due to their high settling velocity, while fine dust particles can undergo long-range transport with an averaged airborne life of 4.3 days.[3,4] Dust events can impact the atmospheric chemistry associated with regional air quality,[5−8] the activity of aerosol cloud condensation nuclei (CCN),[9−11] and the optical properties of aerosols.[12−15]

Airborne dust particles can act as a sink for important gaseous pollutants, such as SO_2, and NO_x.[16−23] For example, the heterogeneous conversion of SO_2 to sulfate on various type of mineral particles (TiO_2, Fe_2O_3, Arizona dust, Gobi Desert dust, and Saharan dust) has been studied.[17,22,24−27] Their reported uptake coefficients of SO_2 onto dust particles vary widely, ranging from 10^{-3} to 10^{-7} (s^{-1}), due to differences in mineral composition, relative humidity (RH), and the type and intensity of light source. Uptake coefficients estimated from laboratory studies have been applied to regional models to simulate the oxidation of SO_2 and NO_2 during dust events. For example, Pozzoli et al.[28] simulated a significant reduction of O_3 and HNO_3 gases in the presence of dust particles using a global model. Wang et al.[29] demonstrated the reduction of O_3 by 9% and SO_2 by 27% using a regional model integrated with heterogeneous chemistry on a dust phase. By implementing the uptake coefficients of major gas species into the community

Received: March 16, 2020
Revised: May 27, 2020
Accepted: June 1, 2020
Published: June 1, 2020

multiscale air quality (CMAQ) model, Dong et al.[30] simulated the sulfate and nitrate formation during a severe dust storm episode in East Asia from March 19 to 21, 2010.

Current regional models approach the heterogeneous chemistry of dusts through a simple first-order uptake of gaseous species, i.e., SO_2 and NO_x. However, the actual dust heterogeneous chemistry proceeds via complex multiphase reactions, including photocatalytic reactions, autoxidation, and buffering of alkaline salts with sulfuric acid or nitric acid in the dust phase. For example, the semiconducting metal oxides in dust particles can be photoactivated and yield electron−hole pairs that further react with water or oxygen molecules on dust surfaces to form oxidizing radicals (i.e., OH radicals).[31,32] SO_2 and NO_x react with these oxidants to form sulfate and nitrate. Thus, heterogeneous photocatalytic oxidation of SO_2 and NO_2 involves second-order reactions and photolysis. To streamline multiphase dust chemistry including photocatalytic oxidation and autoxidation in the chemical transport model, Yu and Jang recently developed the atmospheric mineral aerosol reaction (AMAR) model.[33−35]

In this study, we explored the impact of authentic dust particles on the heterogeneous formation of sulfate and nitrate during the Korea-United States Air Quality (KORUS-AQ) campaign (doi: 10.5067/Suborbital/KORUSAQ/DATA01) performed from May 19 to 30 over across northeastern China, the Korean peninsula, and southern Japan. Mineral dust originating from the Gobi Desert seasonally influences far-East Asia. The AMAR model was implemented in combination with the CAMx model (comprehensive air quality model with extensions) (v6.50, ENVIRON)[36] to simulate the formation of sulfates and nitrates at a regional scale during the dust event of this study. The simulation results were compared with ground-based observational data gathered in the urban area of Seoul, South Korea (Olympic Park, 37.52° N, 127.12° E). To characterize the sensitivity of sulfate and nitrate formation to dust emissions, CAMx-AMAR simulations were performed with different specified emission rates of mineral dust.

METHODOLOGY

Kinetic Mechanisms in AMAR: Heterogeneous Chemistry on Dust Particles. The surfaces of airborne dust particles can act as a sink for gaseous species such as SO_2 and NO_x. During the long-range transport of dust particles, these trace gases can be photocatalytically oxidized on the surface of dust. In this study, the heterogeneous chemistry of SO_2 and NO_x was simulated using the AMAR model.[33,34] In brief, the AMAR model simulates the oxidation of SO_2 and NO_x to form sulfate and nitrate by four pathways: gas-phase oxidation, nondust aqueous reactions,[37] dust-driven autoxidation reactions,[22−24,27,38] and dust-driven photocatalytic reactions.[19,22,27,31−34,39] Dust-driven chemistry is approached by multiphase partitioning of trace gases followed by in-particle chemistry, including autoxidation and photocatalytic oxidation reactions. For example, the autoxidation of SO_2 on the surface of dust occurs in an oxygen environment.

$$SO_2 \xrightarrow{O_2} SO_4^{2-} \quad (1)$$

Under ambient sunlight, the semiconducting metal oxides in the dust (i.e., TiO_2 and Fe_2O_3) are photoactivated to yield electron−hole pairs (e_h), which form radicals (i.e., OH radicals) in the presence of water or oxygen molecules.[31,32] This dust-driven photocatalytic oxidation of SO_2 is described using second-order reactions as follows

$$\text{dust} + \text{photon} \rightarrow \text{dust} + \text{e\_h} \quad (2)$$

$$\text{e\_h} + H_2O \rightarrow {}^{\bullet}OH_{dust} \quad (3)$$

$$\text{e\_h} + O_2 \rightarrow {}^{\bullet}OH_{dust} \quad (4)$$

$$SO_2 + {}^{\bullet}OH_{dust} \rightarrow SO_4^{2-} \quad (5)$$

where ${}^{\bullet}OH_{dust}$ is the OH radical formed on dust surfaces. The photoactivation process of dust particles is parametrized based on the photoactivation rate constant, as described in Section S1 of the Supporting Information.[34] NO_x is oxidized by a similar oxidation pathway as SO_2 in the dust phase. The heterogeneously formed sulfuric acid and nitric acid can react with dust-originated alkaline salts, such as calcium carbonate, to form alkane sulfate and nitrate salts. Hence, the modulation of dust chemical characteristics can change the hygroscopicity of dust particles during long-range transport. Owing to the multiphase heterogeneous chemistry simulated in the AMAR model, the oxidation of SO_2 and NO_2 can be captured under dynamic environmental and meteorological conditions, including sunlight intensity, temperature, and RH.

Integration of AMAR with CAMx. The CAMx regional model encompassed the AMAR model as a subaerosol model to simulate dust heterogeneous chemistry. Sulfuric acid and nitric acid produced through the dust-phase heterogeneous chemistry are partially neutralized with alkaline carbonates in the dust phase. The neutralization reactions were processed until the surface of dust reaches its buffering capacity (3.23×10^{-4} μmol μg^{-1} in Gobi Desert dust particles).[34] Alkaline nitrate was also depleted by the formation of alkaline sulfate. The formation of sulfate and nitrate via aqueous-phase reactions was handled by RADM aqueous chemistry.[40] For gas simulations, the SAPRC-07 mechanism was employed.[41,42]

To process gas−aerosol partitioning of ammonia and nitric acid, dust-phase inorganic species excluding alkaline sulfate and nitrate were then passed to the inorganic thermodynamic model (ISORROPIA).[43] Except for alkaline salts, the total inorganic species originating from the reactions in the dust phase, aqueous phase, and gas phase were included in the ISORROPIA for the calculation of the aerosol ion concentrations, including nitrate and ammonium. Sulfate was predicted in the form of dust-phase sulfate, which is associated with heterogeneous reactions (D- $SO_{4_{pre,hetero}}^{2-}$); gaseous sulfuric acid ($SO_{4_{pre,gas}}^{2-}$); and aqueous-phase sulfate, which is associated with aqueous chemistry ($SO_{4_{pre,aq}}^{2-}$). In addition, D-$SO_{4_{pre,hetero}}^{2-}$ was simulated via three main mechanisms: sulfate (D-$SO_{4_{pre,photo}}^{2-}$) formed through heterogeneously photocatalytic reactions, sulfate (D-$SO_{4_{pre,auto}}^{2-}$) associated with autoxidation, and absorbed gaseous sulfuric acid (D-$SO_{4_{pre,gas}}^{2-}$) that originates from the gas-phase oxidation of SO_2 or primary emissions (i.e., incinerators and coal power plants). In the absence of dust particles, $SO_{4_{pre,gas}}^{2-}$ can be absorbed into pre-existing aqueous aerosols to form $SO_{4_{pre,aq}}^{2-}$. Nitrate, which was semivolatile and relied on gas-particle partitioning, was estimated using total nitrate (T-$NO_{3_{pre}}^{-}$), excluding alkaline nitrate.

The emission of airborne dust particles at the source was generated using WBDUST version 1.1.[44,45] Dust emissions included the fine crustal particle (FCRS, particle diameter:

https://dx.doi.org/10.1021/acsearthspacechem.0c00074
ACS Earth Space Chem. XXXX, XXX, XXX−XXX

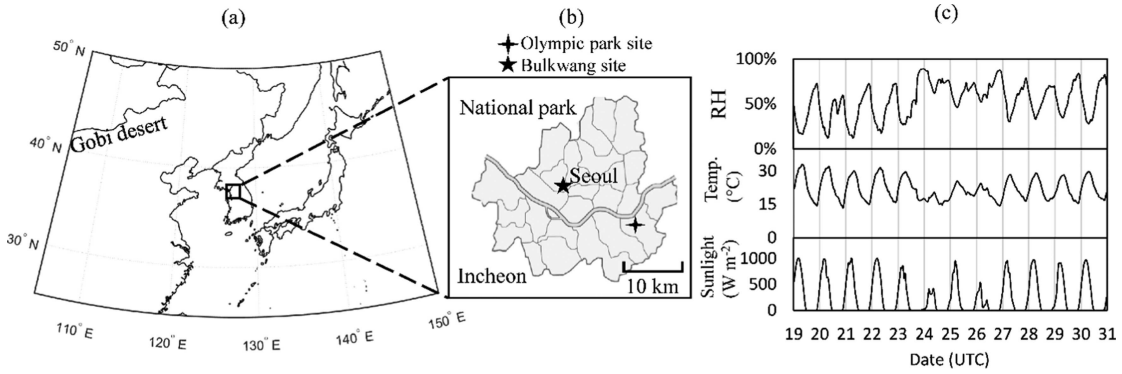

Figure 1. (a) Domain for the simulation of dust chemistry and (b) the ground-based monitoring site during the KORUS-AQ campaign. The Olympic Park sampling site (37.52° N, 127.12° E) is located in the Olympic Park near the urban region of Seoul, Korea and the Bulkwang site (37.61° N, 126.94° E) is located in the same simulation domain. (c) Measured relative humidity (RH, %), temperature (Temp., °C), and sunlight intensity (W m^{-2}) at the Olympic Park site.

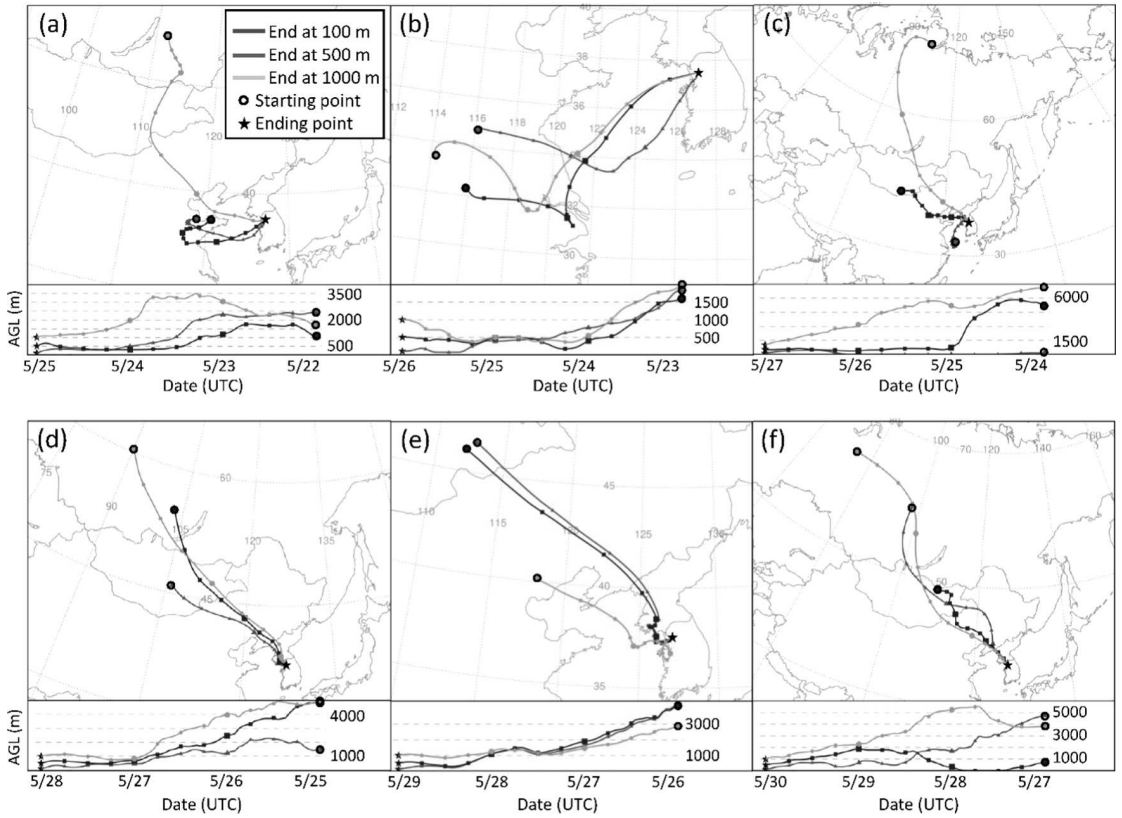

Figure 2. Three-day backward air trajectories for the ground observation site (37.52° N, 127.12° E) during the KORUS-AQ campaign in 2016. The 3-day trajectories were computed using the HYSPLIT model ending at 00:00 (UTC) for (a) May 25, (b) May 26, (c) May 27, (d) May 28, (e) May 29, and (f) May 30. The HYSPLIT trajectory model was developed by National Oceanic and Atmospheric Administration (NOAA). The meteorology input for the simulation was derived using the 0.5° global data assimilation system (GDAS). The vertical velocity of the model was used in the vertical motion calculation method. The simulation was run for three ending heights: 100, 500, and 1000 m above the ground level (AGL).

<2.5 μm) and coarse crustal particle modes (CCRS, particle diameter: 2.5−10 μm). Both FCRS and CCRS were included in the CAMx-AMAR simulation. The total dust mass (TCRS, μg m^{-3}) was then calculated as the sum of FCRS and CCRS. The dust particle with a diameter larger than 10 μm was not considered for the simulation due to its relatively large settling velocity. The CAMx-AMAR simulation was conducted using grids with a 27-km resolution nested with 22 vertical layers. Figure 1 shows the simulation domain over northeastern China, the Korean peninsula, and southern Japan. To predict the concentrations of chemical species at the specific sampling site, the predicted concentrations of the chemical species were processed using the inverse distance weighting method (IDW).

Ground-Based Observations during the KORUS-AQ Campaign. Ground-level observational data were performed at a monitoring station located in the Olympic Park, Seoul, South Korea (37.52° N, 127.12° E) and the Bulkwang site (37.61° N, 126.94° E). The field data for this study was

https://dx.doi.org/10.1021/acsearthspacechem.0c00074
ACS Earth Space Chem. XXXX, XXX, XXX−XXX

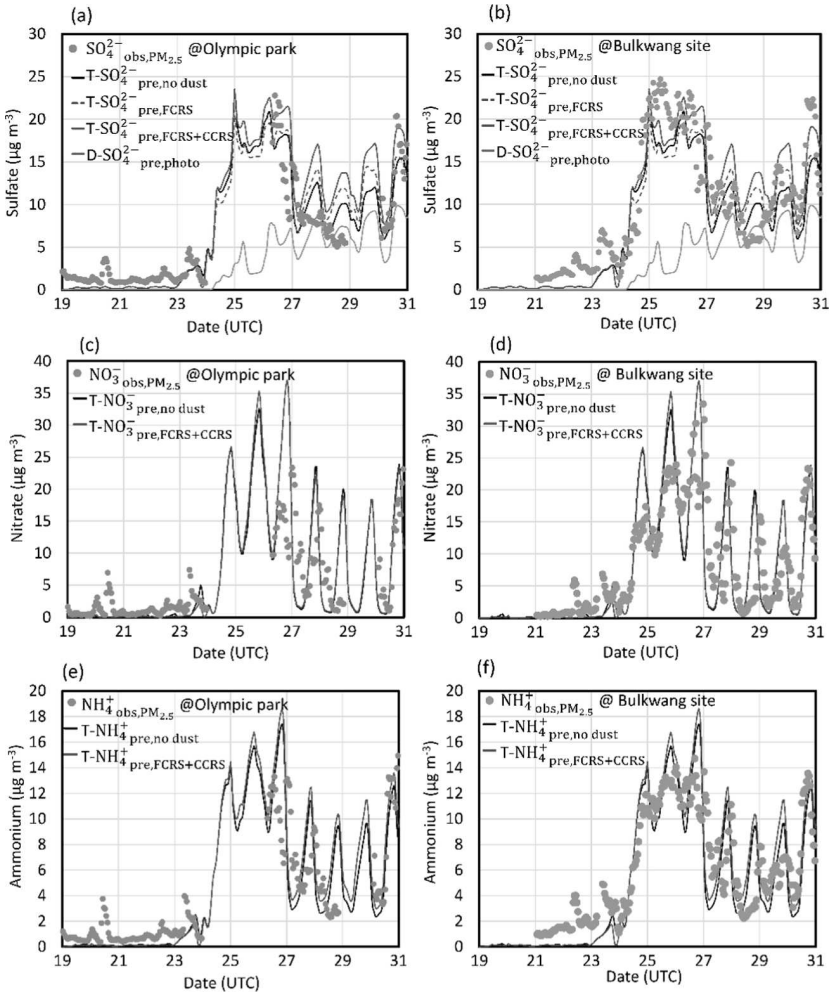

Figure 3. Observed sulfate ($SO_{4_{obs,PM2.5}}^{2-}$) vs simulated sulfate (T-$SO_{4_{pre}}^{2-}$) under different conditions: sulfate without dust emissions (T-$SO_{4_{pre,no\ dust}}^{2-}$), sulfate with fine crustal particles (T-$SO_{4_{pre,FCRS}}^{2-}$), and sulfate with both fine and coarse crustal particles (T-$SO_{4_{pre,FCRS+CCRS}}^{2-}$) from May 19 to 30 at the monitoring sites: (a) Olympic Park site and (b) Bulkwang site. D-$SO_{4_{pre,photo}}^{2-}$ represents the sulfate formed by heterogeneously photocatalytic reaction. Measured nitrate ($NO_{4_{obs,PM2.5}}^{2-}$) vs simulated nitrate under two conditions: nitrate without dust emissions (T-$NO_{3_{pre,no\ dust}}^{-}$) and nitrate with both FCRS and CCRS particles (T-$NO_{3_{pre,FCRS+CCRS}}^{-}$) at two sites: (c) Olympic Park site and (d) Bulkwang site. Measured ammonium ($NH_{4_{obs,PM2.5}}^{+}$) vs simulated ammonium under two conditions: ammonium without dust emissions (T-$NH_{4_{obs,no\ dust}}^{+}$) and ammonium with both FCRS and CCRS particles (T-$NH_{4_{pre,FCRS+CCRS}}^{+}$) at two sites: (e) Olympic Park site and (f) Bulkwang site.

provided by the National Institute of Environmental Research (NIER, Korea). The water-soluble inorganic ion concentrations (sulfate, nitrate, and ammonium) in $PM_{2.5}$ were monitored every hour using the Monitor for AeRosols and Gases in Ambient air (MARGA ADI 2080, Metrohm, Switzerland). Water-soluble ion data obtained from the Olympic Park site were available for the time period of May 19 (0 UTC)−May 24 (0 UTC), May 26 (0 UTC)−May 29 (0 UTC), and May 30 (0 UTC)−May 31 (0 UTC). The mass concentrations of $PM_{2.5}$ and PM_{10} were continuously sampled using a particulate monitor (FH62C14, Thermo) and averaged every hour. The observations for $PM_{2.5}$ and PM_{10} are presented in Figure S1. The gas concentrations of O_3, NO_x, and SO_2 were measured using an O_3 analyzer (EC9810, Ecotech, Australia), a NO_x analyzer (EC9841, Ecotech, Australia), and a SO_2 analyzer (EC9850, Ecotech, Australia), respectively. The observational data for gaseous species is presented in Figure S2. The relative humidity (RH), temperature (°C), and sunlight radiation (W m^{-2}) were monitored using a hydrometer (083D-1−35 T/RH Sensor, Met One Instruments, Inc.) and a solar radiation sensor (096−1, Met One Instruments, Inc.) and are presented in Figure 1c. The errors associated with the water-soluble ion concentrations, the concentration of PM, the concentration of gaseous species, RH, temperature, and sunlight radiation were ±10%, ±1 μg m^{-3}, ±5%, ±2%, ±0.15 °C, and ±3%, respectively.

Trajectory of the Dust Parcels. The sources of long-range-transported mineral dust for our study domain include two primary regions: the Gobi Desert (northern China and southern Mongolia) and the Taklimakan Desert (mid-West China). Dust particles from the Gobi Desert can be entrained to altitudes less than 3000 m. The Gobi Desert is one of the dominant sources of dust particles for East Asia[46] and western North America.[47−49] To evaluate the spatiotemporal patterns of airmass transport, 3-day backward trajectories were computed every 24 h from May 25 to 30, 2016, using the HYSPLIT trajectory model[50] developed by the National Oceanic and Atmospheric Administration (NOAA) (Figure

https://dx.doi.org/10.1021/acsearthspacechem.0c00074
ACS Earth Space Chem. XXXX, XXX, XXX−XXX

2). The meteorology input for the calculation of trajectories was the global data assimilation system (GDAS), which has a resolution of 0.5° × 0.5°. To predict the long-range transport of dust-containing air parcels in regional scales within the boundary layer (<∼1 km), the trajectories of the air parcel were simulated for three different altitudes (100, 500, and 1000 m above ground) at the Olympic Park site (37.52° N, 127.12° E).

■ RESULTS AND DISCUSSION

Simulated Sulfate and Nitrate Using CAMx-AMAR. Sulfate, nitrate, and ammonium concentrations were simulated using CAMx-AMAR and plotted vs ground-based data from the Olympic Park monitoring site and the Bulkwang site from May 19 to 30, 2016 during the KORUS-AQ campaign. In CAMx-AMAR, total sulfate (T-$SO_{4_{pre}}^{2-}$) was simulated for three different dust conditions, as seen in Figure 3a: sulfate without dust emission data (T-$SO_{4_{pre,no\ dust}}^{2-}$), sulfate with emission data from FCRS (T-$SO_{4_{pre,FCRS}}^{2-}$), and sulfate with emission data from both FCRS and CCRS (T-$SO_{4_{pre,FCRS+CCRS}}^{2-}$). The ground-based observed sulfate ($SO_{4_{obs,PM2.5}}^{2-}$) was simulated against T-$SO_{4_{pre,FCRS}}^{2-}$ because field data include the ion concentrations associated with $PM_{2.5}$. The concentrations of $SO_{4_{obs,PM2.5}}^{2-}$ were noticeably high during May 25−27 and May 30−31 when dust mass loadings were high (Figure S1). The model accurately simulates this tendency as well as the sulfate concentrations. The simulated sulfate was mainly contributed by the sulfate associated with dust particles in the FCRS mode because CCRS particles settled quickly during long-range transport. Without dust-phase reactions (in the absence of dust emission data), sulfate was underestimated by 20−30% when dust loads were high ($SO_{4_{obs,PM2.5}}^{2-}$ vs $SO_{4_{pre,no\ dust}}^{2-}$ in Figure 3a,b). As seen in $SO_{4_{obs,PM2.5}}^{2-}$ (Figure 3a,b) and in the sunlight intensity profiles (Figure 1c), high $SO_{4_{obs,PM2.5}}^{2-}$ appeared in the late afternoons (May 26 and May 30). These high sulfate concentrations were also correctly simulated by the model. The simulated D-$SO_{4_{pre,photo}}^{2-}$ was relatively sensitive to the sunlight intensity and continuously increased during the day. For May 27, sulfate concentration was overestimated at the Olympic Park site, but it was well simulated at the Bulkwang site. The overestimation of sulfate could be related to the spatial resolution between the observation site and the simulation domain.

Figure 3c,d illustrates the total concentrations of particulate nitrate at the Olympic Park site and the Bulkwang site, respectively. Figure 3e,f shows the total particulate ammonium at two sites, respectively. Compared with sulfate, the CAMx-AMAR model better simulated both nitrate and ammonium during the sampling period. The high concentrations of nitrate and ammonium ions on May 26, 27, and 30 were well simulated by the model. Both the observations and simulations demonstrated that nitrate and ammonium were sensitive to RH and temperature, with a diurnal pattern (Figure 1c): high RH and low temperatures at night and low RH and high temperatures during the day. Recent studies by Yu and Jang[34] demonstrated that both RH and temperature were important to the formation of nitrate and sulfate on dust particles. The gas-dust partitioning coefficients of SO_2, NO_2, and nitric acid increase with decreasing temperatures. At a high RH, the increased aqueous layer on dust particles promotes the gas-dust partitioning process of hydrophilic gases. Dust-phase nitrate is dominated by partitioned nitric acid and its neutralization with ammonia because dust surfaces are buffered with sulfate, as discussed above. It should be noted that the high concentration of particulate nitrate appeared only when sulfuric acid, a strong nonvolatile acid, was fully neutralized by dust salts or ammonia. The nitric acid that accumulates in the gas phase via a reaction with NO_2 with an OH radical was rapidly partitioned to hygroscopic dust surfaces in the morning. However, nitric acid offgasses from dust particles when the temperature increased, and RH decreased. Hence, both nitrate and ammonium reached a daily maximum in the early morning, as seen in Figure 3c,d, respectively. In particular, the maximum concentrations of nitrate and ammonium were high between May 24 and 26 when RH was high, and the temperature was low (Figure 1c). To characterize the impact of dust particles on nitrate formation, the model simulation was also performed without the input of dust emission data. Unlike sulfate, the difference in the simulated nitrate concentrations between the absence and presence of dust emission was negligible because nitric acid formation was dominated by the gas-phase oxidation of NO_2. In the absence of dust particles, gaseous nitric acid will partition into sulfate seeded aqueous particles. Ammonium concentrations can be affected by both sulfate and nitrate.

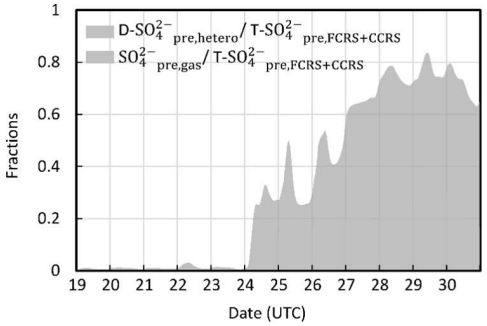

Figure 4. Fraction of simulated sulfate associated with the dust-phase heterogeneous chemistry (D-$SO_{4_{pre,hetero}}^{2-}$/T-$SO_{4_{pre,FCRS+CCRS}}^{2-}$) and that associated with gaseous sulfuric acid ($SO_{4_{pre,gas}}^{2-}$/T-$SO_{4_{pre,FCRS+CCRS}}^{2-}$) at the Olympic Park site.

Figure 4 illustrates the fraction of the heterogeneously formed sulfate (D-$SO_{4_{pre,hetero}}^{2-}$), contributing to total sulfate (T-$SO_{4_{pre,FCRS+CCRS}}^{2-}$). During high dust loads, D-$SO_{4_{pre,FCRS+CCRS}}^{2-}$ contributed to approximately 60% of total sulfate, and gaseous sulfuric acid ($SO_{4_{pre,gas}}^{2-}$) contributed to approximately 20%. In the presence of dust particles, gaseous sulfuric acid is immediately taken up by the dust particles and forms D-$SO_{4_{pre,gas}}^{2-}$. During the same time period, when dust loads were high, sulfate formation via aqueous reactions was significantly suppressed (up to 66%) due to the competition between dust particles and the aqueous phase of the gas-particle partitioning of SO_2. In the simulation, D-$SO_{4_{pre,hetero}}^{2-}$ is partially attributable to the sulfate-buffered alkaline salts (i.e., calcium sulfate) produced from the reaction of sulfuric acid with alkaline carbonates. Our simulation suggested that dust particles were heavily coated with sulfate, overcoming the buffering capacity of dust. The excess amount of sulfuric acid on dust particles

https://dx.doi.org/10.1021/acsearthspacechem.0c00074
ACS Earth Space Chem. XXXX, XXX, XXX−XXX

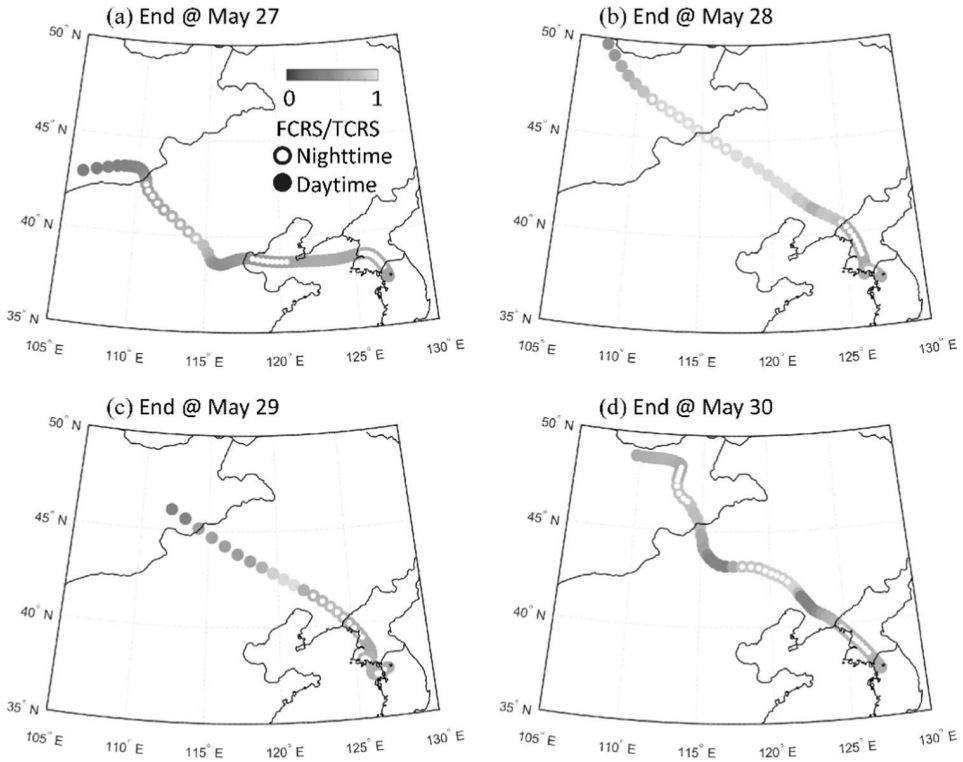

Figure 5. One-hour average mass ratio of fine crustal dust particles (FCRS) to total dust mass (TCRS) along the four different 3-day back trajectories ended at 500 m AGL for (a) May 27, (b) May 28, (c) May 29, and (d) May 30.

was partially or fully neutralized by ammonia in the East Asian atmosphere, where ammonia concentrations are relatively high.

Observed gaseous species, such as SO_2, NO_x, and O_3, are shown in Figure S2. The CAMx-AMAR model accurately predicted the O_3 concentration but underestimated the SO_2 and NO_x concentrations ranging from 52 to 84%. The deviation between the simulation in regard to SO_2 and NO_x and observational data may be associated with missing local emissions.

Chemical Compositions during the Long-range Transport of Dust Particles. Airborne dust particles originating from the Gobi Desert undergo long-range transport and eventually reach a remote region in East Asia and the west coast of North America.[47−49] Due to the rapid deposition rates of CCRS particles, the spatial distribution of dust mass is dominated by FCRS. Figure 5 shows that the simulated mass ratio of FCRS to TCRS along the back trajectories ended at 0:00 UTC from May 27 to 30, 2016. For all simulations, the fraction ratios of FCRS to TCRS are greater than 0.6 when dust particles approached the Korean peninsula. As shown in Figure S1, the observed particulate matter at the ground-based observation site is dominated by $PM_{2.5}$, which also supports our simulation results showing that the long-range-transported dust particles are mainly in the fine mode. During the KORUS-AQ campaign, the simulated ground-level concentrations of dust particles reached up to 30 μg m^{-3} over downwind areas, such as East China and the Korean peninsula. According to the simulated back trajectories, the average travel time for dust parcels was less than 3 days from the source region to the sampling site. This is a sufficient amount of time for dust particles to impact the regional air quality of East Asia for 3 days, especially during the dust storm season; however, the travel times simulated in this study are somewhat shorter than the previously reported lifetime of fine airborne dust particles (approximately 4.3 days).[3,S1]

The observed field data during the KORUS-AQ campaign demonstrated that the long-range transport of heavy aerosol plumes from East-Central China to the Korean peninsula significantly impacts regional air quality.[S2,S3] To characterize the impact of dust particles on aerosol compositions during long-range transport, the HYSPLIT trajectory model was employed. Figure 6 illustrates the simulated concentrations of chemical species (dust mass, sulfate, and nitrate in Figure 6a−f) and meteorological variables (the intensity of solar radiation, temperature, and water vapor concentration in Figure 6g−i). The 3-day back trajectories of the air parcel, originating in the Gobi Desert and arriving at the ground-based air monitoring site of this study on May 27, 2016 (UTC), were computed for 500 m AGL (Figure 2c). The daily averaged ground-level concentrations of chemical species (sulfate, nitrate, ammonium, SO_2, and dust mass) and meteorological variables (temperature and water vapor) were simulated between May 21 and 29, as shown in Figures S3−S9.

Dust mass concentrations were high near the source region on May 24, 2016 and gradually decreased due to the deposition of dust particles during transport (Figure 6a). Figure 6b and 6c illustrate the concentration of T-$SO^{2-}_{4,\mathrm{pre,FCRS+CCRS}}$ and T-$NO^{-}_{3,\mathrm{pre,FCRS+CCRS}}$, respectively. T-$SO^{2-}_{4,\mathrm{pre,FCRS+CCRS}}$ was low between May 24 and 26, and slowly increased when the air parcel transited the Yellow Sea. The SO_2 concentrations were high in the industrial areas near the Chinese coast (Figure S6), but high sulfate concentrations appeared in the downwind region (more than 24 h travel of the air parcel from the industrial regions). Within this air parcel trajectory, the intensity of solar radiation (Figure 6d) was high on May 26 and promoted photochemical reactions of chemical species in

https://dx.doi.org/10.1021/acsearthspacechem.0c00074
ACS Earth Space Chem. XXXX, XXX, XXX−XXX

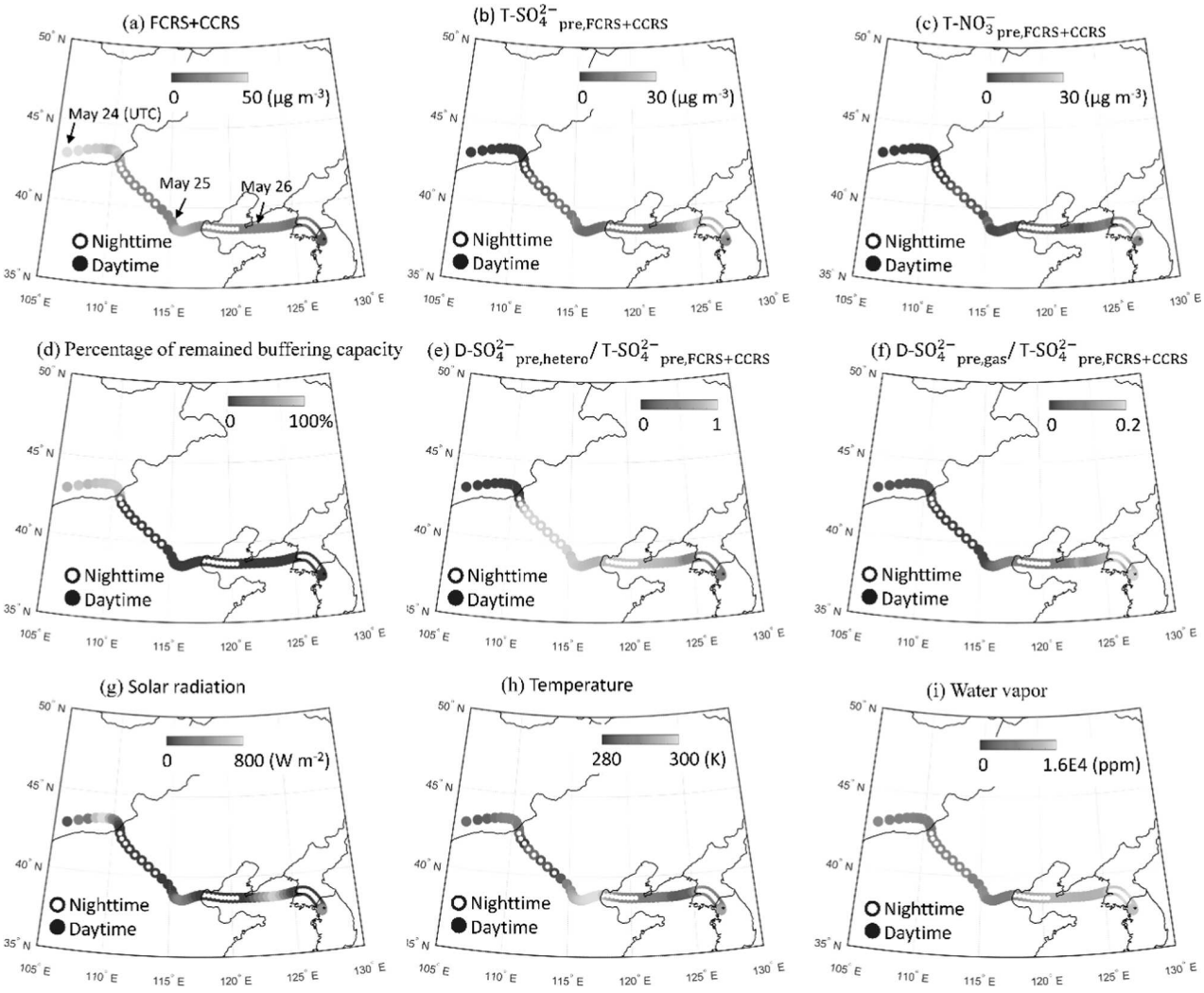

Figure 6. Trajectories of the simulated 1 h average chemical species and meteorological variables: (a) total dust mass concentrations (FCRS + CCRS), (b) total sulfate ($T\text{-}SO_{4\,pre,FCRS+CCRS}^{2-}$), (c) total nitrate ($T\text{-}NO_{3\,pre,FCRS+CCRS}^{-}$), (d) percentage of the available dust-buffering capacity, (e) ratio of heterogeneously formed sulfate ($D\text{-}SO_{4\,pre,hetero}^{2-}$) to $T\text{-}SO_{4\,pre,FCRS+CCRS}^{2-}$, (f) ratio of gaseous sulfuric acid ($D\text{-}SO_{4\,pre,gas}^{2-}$) to ($T\text{-}SO_{4\,pre,FCRS+CCRS}^{2-}$), (g) intensity of solar radiation (W m^{-2}), (h) temperature (K), and (i) water vapor concentrations (ppm). The simulated concentrations of chemical species are plotted on the 3-day backward air trajectory ending at 00:00 May 27, 2016 (UTC) for 500 m AGL. The open circle represents the nighttime simulation (from sunset to sunrise) and the closed circle represents the daytime simulation.

all phases (gas phase, aqueous phase, and dust surface). The buffering capacity of mineral dust particles was simulated on the trajectory (Figure 6d). Dust particles were rapidly buffered by sulfate within 12 h of entering inland China. We conclude that the neutralization capacity of dust particles in East Asia originating from the Gobi Desert is mostly saturated.

The fraction of heterogeneously formed sulfate to total sulfate ($D\text{-}SO_{4\,pre,hetero}^{2-}/T\text{-}SO_{4\,pre,FCRS+CCRS}^{2-}$) and that of gaseous sulfuric acid to total sulfate ($D\text{-}SO_{4\,pre,gas}^{2-}/T\text{-}SO_{4\,pre,FCRS+CCRS}^{2-}$) are shown in Figure 6e and 6f, respectively. The contribution of dust heterogeneous reactions to total sulfate was high (>0.9) near the dust source region but gradually declined as dust particles were deposited. The value of $D\text{-}SO_{4\,pre,hetero}^{2-}/T\text{-}SO_{4\,pre,FCRS+CCRS}^{2-}$ was approximately 0.6 when dust parcels arrived at the ground-based monitoring site at Seoul, South Korea on May 27, 2016. The fraction of gaseous sulfuric acid to total sulfate (Figure 6f) increased due to the reduction in dust mass and the increased primary emissions of sulfuric acid when air parcels moved from the Yellow Sea to the Korean peninsula.

In addition to sunlight intensity, particulate nitrate can be significantly influenced by temperature and humidity through gas-particle partitioning of NO_2 and nitric acid. Nitric acid was abundant in urban and industrial areas in China and intruded the dust air parcels during the day on May 25, 2016. At night, when the air parcel moved from inland China to the Yellow Sea, temperatures decreased (from 300 to 285 K) and humidity increased over the ocean, as seen in Figure 6h, and 6i. This meteorological condition was favorable for the formation of particulate nitrate. The simulated $T\text{-}NO_{3\,pre,FCRS+CCRS}^{-}$ in Figure 6c continuously increased through the night on May 26, 2016. This accumulation of hygroscopic nitrate on dust particles may possibly promote heterogeneous uptake of gaseous chemical species, such as SO_2.[34,54−56]

The proton concentrations in air parcels were simulated based on the mass balance of ion species, excluding the sulfate associated with dust-buffering reactions. As seen in Figure

https://dx.doi.org/10.1021/acsearthspacechem.0c00074
ACS Earth Space Chem. XXXX, XXX, XXX−XXX

S10a, the dust parcel becomes acidic over the Yellow Sea, where ammonia was limited (Figure S10b) and photochemical reactions were active (Figure 6g). As the parcel approached the Korean peninsula, the acidity of the aerosols immediately decreased by gaining ammonia sourced from human activities, neutralizing acidic sulfate. Interestingly, $T\text{-}NO_{3,pre,FCRS+CCRS}^{-}$ (Figure 6c) reached a maximum after the particulate proton declined because aerosol acidity hinders the partitioning of nitric acid.

Sensitivity of Heterogeneous Chemistry to Dust Emission. The dust mass concentrations observed during the KORUS-AQ campaign were relatively lower than those in typical spring dust events, although they were higher than the dust concentrations observed during nondust seasons. To understand the impact of dust particles on the formation of atmospheric sulfate and nitrate, the model was simulated with dust mass 2 times greater than the field data of this study. In Figure S11a, the sulfate concentrations on the back trajectories ending at 0:00 of May 27, 2016 (UTC) were simulated with double the mass of dust emissions. With an increase in the dust load compared to that shown in Figure 6b, a large area including inland China, the Yellow Sea, and the Korean peninsula can be impacted by the high sulfate associated with dust particles from the Gobi Desert. The enhancement of sulfate formation given a higher dust load was also reported by recent chamber studies.[22,27] When the dust load was doubled, the simulated $D\text{-}SO_{4,pre,hetero}^{2-}/T\text{-}SO_{4,pre,FCRS+CCRS}^{2-}$ increased from 67.3 to 78.7% (Figures 6e and S11b) at the ground-based air monitoring site, indicating the importance of dust-driven sulfate formation during dust events. Unlike sulfuric acid, sulfated acidic dust particles drive nitric acid to the protonated states and then into the gas-phase (Figure S11c) due to its high volatility.[34,57]

Uncertainties and Atmospheric Implications. The major model uncertainties associated with the simulation of the heterogeneous chemistry on dust is originated from both the model parameters in the AMAR and the dust emissions, which is estimated with the WBDUST model. In the AMAR model, the photoactivation rate constant of dust particles and the hygroscopicity parameters are obtained using the authentic mineral dust collected from the northern Gobi Desert.[34] The dust compositions, however, can be diverse depending upon dust sources that originate from different areas in the Gobi Desert and they can influence heterogeneous chemistry on dust. Therefore, the parameters associated with dust's heterogeneous chemistry in AMAR may not characterize the actual dust properties during dust storm events. Additionally, a large variation also appeared in dust emission data (~50%).[44,45] The predicted dust emissions can be changed with meteorological conditions, the land coverage, and the clay content. Due to coagulation, dust particles can also scavenge small particles such as sulfate aerosols created by SO_2 aqueous reactions. In this study, the coagulation process between particles was not included because dust particles mainly comprised FCRS particles during long-range transport. These fine dust particles have a relatively slow coagulation rate with submicron aqueous particles.

Airborne dust particles promote the heterogeneous oxidation of gaseous species, such as NO_2 and SO_2, through both photocatalytic reactions and the autoxidation pathway. In the presence of dust particles, the estimated sulfate concentration was enhanced by up to 29% (Figure 3a,b) at the ground-based monitoring site of this study. Figure S12 illustrates satellite images of the simulated domains between May 21 and 29 from a moderate-resolution imaging spectroradiometer (MODIS) onboard NASA's Aqua satellite (source: https://worldview.earthdata.nasa.gov/). However, no clear transport of dust plumes appeared in the satellite images during the KORUS-AQ campaign, which was not performed in the typical dust season during spring months (between February and April). A higher dust mass load during the dust season may lead to enhanced sulfate formation in the regions downwind from the dust source. For example, Wang et al.[58] observed that the fraction of sulfate to calcium and the fraction of nitrate to calcium were significantly elevated during a super Asian dust storm in March 2010. In addition, SO_2 emissions seasonally increase during the cold season due to heating demand. In spring, SO_2 emissions are still high and can rapidly increase sulfate during a dust outbreak. In our simulation, dust particles were fully buffered when air parcels entered inland China, where anthropogenic air pollutants are abundant (Figure 6d). The sulfate on dust particles significantly surpassed the sulfate-associated buffering capacity (buffered sulfate was 2−5% of total sulfate). Thus, the impact of dust-buffered sulfate on aerosol acidity may be negligible. Over urban areas, the predicted aerosol proton concentration ranged from 10^{-5} to 10^{-3} μmol m^{-3}. The high aerosol acidity in the dust parcels appeared over the Yellow Sea downstream from industrial areas (Figure S10a) due to sulfate formation in the dust phase under ammonia-poor environments (limited ammonia sources over the ocean). The aerosol acidities over the Yellow Sea were 1 order of magnitude higher than those in upstream industrial areas. In addition, dust plumes would possibly interact with sea spray aerosol and deplete chloride ions in it (neutralization of aerosol acidity) during the transportation over the ocean and coastal areas. The effect of sea spray aerosol on dust's heterogeneous chemistry needs to be explored in future.

The CCN activities of particulate matter during dust events may be modulated. For example, the reduced formation of sulfate via nondust aqueous aerosol can suppress the CCN activity during dust episodes, but the hygroscopicity of aged dust can increase the CCN activity due to coating with hygroscopic nitrate salts.[10,59] In addition, large dust particles can compete with nondust submicron particles for water vapor and potentially reduce the CCN activity.[9,60,61]

In recent years, there has been an increasing concern regarding reducing SO_2 emissions. For example, global SO_2 emissions were reduced by 31% from 1990 to 2015[62] and by 88% in North America from 1990 to 2018 (https://www.epa.gov/air-emissions-inventories/air-pollutant-emissions-trends-data). Zhang et al.[63] estimated that there was a large reduction of SO_2 emission (~62%) in China between 2010 and 2017. With these trends, the formation of particulate sulfate has been reduced, and nitrate has become relatively important in the composition of particulate. Consequently, dust particles can be coated with hygroscopic nitrate salts, such as calcium nitrate and ammonium nitrate. Additionally, organic species can also interact with dust particles.[64−67] For example, semivolatile organic compounds can be heterogeneously oxidized on a dust surface and the carboxylic acid group can produce carboxylate salts in the dust. Regional models need to be improved through future studies to predict the heterogeneous chemistry of hydrocarbons on dust and their impact on nitrate and sulfate formation.

https://dx.doi.org/10.1021/acsearthspacechem.0c00074
ACS Earth Space Chem. XXXX, XXX, XXX−XXX

■ ASSOCIATED CONTENT

Supporting Information

The Supporting Information is available free of charge at https://pubs.acs.org/doi/10.1021/acsearthspacechem.0c00074.

Photoactivation parameters to form dust-phase oxidants in Gobi Desert dust particles (Section S1), ground-based observations vs model simulation at the Olympic Park (Section S2), time profiles of observed $PM_{2.5}$ and PM_{10} at the ground-level monitoring site in the Olympic Park (Figure S1),and time profiles of simulated and observed data at the ground-level monitoring site in the Olympic Park (Figure S2) (PDF)

■ AUTHOR INFORMATION

Corresponding Author

Myoseon Jang − *Department of Environmental Engineering Sciences, University of Florida, Gainesville, Florida 32611, United States;* orcid.org/0000-0003-4211-7883; Phone: +1-352-846-1744; Email: mjang@ufl.edu

Authors

Zechen Yu − *Department of Environmental Engineering Sciences, University of Florida, Gainesville, Florida 32611, United States;* orcid.org/0000-0002-6763-0520

Soontae Kim − *Department of Environmental Engineering, Ajou University, Suwon-si 16499, South Korea;* orcid.org/0000-0002-1198-934X

Changhan Bae − *Department of Environmental Engineering, Ajou University, Suwon-si 16499, South Korea;* orcid.org/0000-0003-3347-4328

Bonyoung Koo − *Bay Area Air Quality Management District, San Francisco, California 94105, United States*

Ross Beardsley − *Ramboll USA, Novato, California 94945, United States*

Jinsoo Park − *Air Quality Research Division, Environmental Research Complex, Seoul 06744, South Korea*

Lim Seok Chang − *Air Quality Research Division, Environmental Research Complex, Seoul 06744, South Korea*

Hee Choon Lee − *National Institute of Meteorological Sciences, Seogwipo-si 63568, South Korea*

Yun-Kyu Lim − *National Institute of Meteorological Sciences, Seogwipo-si 63568, South Korea*

Jeong Hoon Cho − *National Institute of Meteorological Sciences, Seogwipo-si 63568, South Korea*

Complete contact information is available at: https://pubs.acs.org/10.1021/acsearthspacechem.0c00074

Notes

The authors declare no competing financial interest.

■ ACKNOWLEDGMENTS

This research was supported financially by the National Institute of Metrological Sciences (KMA2018-00512), the Ministry of Science and ICT, the Ministry of Environment, the Ministry of Health and Welfare (2017M3D8A1090654), the National Science Foundation (NSF#1923651), and the Fulbright Scholarship (from USA to Mongolia). The authors also thank Chris Emery from Ramboll USA, Inc. (CA) for supporting the set up of CAMx simulation.

■ REFERENCES

(1) Textor, C.; Schulz, M.; Guibert, S.; Kinne, S.; Balkanski, Y.; Bauer, S.; Berntsen, T.; Berglen, T.; Boucher, O.; Chin, M.; Dentener, F.; Diehl, T.; Easter, R.; Feichter, H.; Fillmore, D.; Ghan, S.; Ginoux, P.; Gong, S.; Grini, A.; Hendricks, J.; Horowitz, L.; Huang, P.; Isaksen, I.; Iversen, I.; Kloster, S.; Koch, D.; Kirkevåg, A.; Kristjansson, J. E.; Krol, M.; Lauer, A.; Lamarque, J. F.; Liu, X.; Montanaro, V.; Myhre, G.; Penner, J.; Pitari, G.; Reddy, S.; Seland, Ø.; Stier, P.; Takemura, T.; Tie, X. Analysis and Quantification of the Diversities of Aerosol Life Cycles within AeroCom. *Atmos. Chem. Phys.* **2006**, *6*, 1777−1813.

(2) Peng, Y.; von Salzen, K.; Li, J. Simulation of Mineral Dust Aerosol with Piecewise Log-normal Approximation (PLA) in CanAM4-PAM. *Atmos. Chem. Phys.* **2012**, *12*, 6891−6914.

(3) Zender, C. S.; Miller, R. L. R. L.; Tegen, I. Quantifying Mineral Dust Mass Budgets:Terminology, Constraints, and Current Estimates. *EOS, Trans., Am. Geophys. Union* **2004**, *85*, 509−512.

(4) Scheuvens, D.; Schutz, L.; Kandler, K.; Ebert, M.; Weinbruch, S. Bulk Composition of Northern African Dust and Its Source Sediments—A Compilation. *Earth-Sci. Rev.* **2013**, *116*, 170−194.

(5) Zheng, B.; Zhang, Q.; Zhang, Y.; He, K. B.; Wang, K.; Zheng, G. J.; Duan, F. K.; Ma, Y. L.; Kimoto, T. Heterogeneous chemistry: a mechanism missing in current models to explain secondary inorganic aerosol formation during the January 2013 haze episode in North China. *Atmos. Chem. Phys.* **2015**, *15*, 2031−2049.

(6) Xue, J.; Yuan, Z.; Griffith, S. M.; Yu, X.; Lau, A. K.; Yu, J. Z. Sulfate Formation Enhanced by a Cocktail of High NO_x, SO_2, Particulate Matter, and Droplet pH during Haze-Fog Events in Megacities in China: An Observation-Based Modeling Investigation. *Environ. Sci. Technol.* **2016**, *50*, 7325−7334.

(7) Wang, G. H.; Zhang, R. Y.; Gomez, M. E.; Yang, L. X.; Zamora, M. L.; Hu, M.; Lin, Y.; Peng, J. F.; Guo, S.; Meng, J. J.; Li, J. J.; Cheng, C. L.; Hu, T. F.; Ren, Y. Q.; Wang, Y. S.; Gao, J.; Cao, J. J.; An, Z. S.; Zhou, W. J.; Li, G. H.; Wang, J. Y.; Tian, P. F.; Marrero-Ortiz, W.; Secrest, J.; Du, Z. F.; Zheng, J.; Shang, D. J.; Zeng, L. M.; Shao, M.; Wang, W. G.; Huang, Y.; Wang, Y.; Zhu, Y. J.; Li, Y. X.; Hu, J. X.; Pan, B.; Cai, L.; Cheng, Y. T.; Ji, Y. M.; Zhang, F.; Rosenfeld, D.; Liss, P. S.; Duce, R. A.; Kolb, C. E.; Molina, M. J. Persistent sulfate formation from London Fog to Chinese haze. *Proc. Natl. Acad. Sci. U.S.A.* **2016**, *113*, 13630−13635.

(8) Pan, X. L.; Uno, I.; Wang, Z.; Nishizawa, T.; Sugimoto, N.; Yamamoto, S.; Kobayashi, H.; Sun, Y. L.; Fu, P. Q.; Tang, X.; Wang, Z. F. Real-time observational evidence of changing Asian dust morphology with the mixing of heavy anthropogenic pollution. *Sci. Rep.* **2017**, *7*, No. 335.

(9) Karydis, V. A.; Tsimpidi, A. P.; Bacer, S.; Pozzer, A.; Nenes, A.; Lelieveld, J. Global Impact of Mineral Dust on Cloud Droplet Number Concentration. *Atmos. Chem. Phys.* **2017**, *17*, 5601−5621.

(10) Gaston, C. J.; Pratt, K. A.; Suski, K. J.; May, N. W.; Gill, T. E.; Prather, K. A. Laboratory Studies of the Cloud Droplet Activation Properties and Corresponding Chemistry of Saline Playa Dust. *Environ. Sci. Technol.* **2017**, *51*, 1348−1356.

(11) Kanji, Z. A.; Sullivan, R. C.; Niemand, M.; DeMott, P. J.; Prenni, A. J.; Chou, C.; Saathoff, H.; Mohler, O. Heterogeneous ice nucleation properties of natural desert dust particles coated with a surrogate of secondary organic aerosol. *Atmos. Chem. Phys.* **2019**, *19*, 5091−5110.

(12) Ryder, C. L.; Highwood, E. J.; Rosenberg, P. D.; Trembath, J.; Brooke, J. K.; Bart, M.; Dean, A.; Crosier, J.; Dorsey, J.; Brindley, H.; Banks, J.; Marsham, J. H.; McQuaid, J. B.; Sodemann, H.; Washington, R. Optical properties of Saharan dust aerosol and contribution from the coarse mode as measured during the Fennec 2011 aircraft campaign. *Atmos. Chem. Phys.* **2013**, *13*, 303−325.

(13) Ridley, D. A.; Heald, C. L.; Kok, J. F.; Zhao, C. An observationally constrained estimate of global dust aerosol optical depth. *Atmos. Chem. Phys.* **2016**, *16*, 15097−15117.

(14) Spyrou, C. Direct radiative impacts of desert dust on atmospheric water content. *Aerosol Sci. Technol.* **2018**, *52*, 693−701.

https://dx.doi.org/10.1021/acsearthspacechem.0c00074
ACS Earth Space Chem. XXXX, XXX, XXX−XXX

(15) Huang, K.; Fu, J. S.; Lin, N. H.; Wang, S. H.; Dong, X. Y.; Wang, G. C. Superposition of Gobi Dust and Southeast Asian Biomass Burning: The Effect of Multisource Long-Range Transport on Aerosol Optical Properties and Regional Meteorology Modification. *J. Geophys. Res.: Atmos.* **2019**, *124*, 9464−9483.
(16) Mogili, P. K.; Kleiber, P. D.; Young, M. A.; Grassian, V. H. Heterogeneous Uptake of Ozone on Reactive Components of Mineral Dust Aerosol: An Environmental Aerosol Reaction Chamber Study. *J. Phys. Chem. A* **2006**, *110*, 13799−13807.
(17) Usher, C. R.; Al-Hosney, H.; Carlos-Cuellar, S.; Grassian, V. H. A Laboratory Study of the Heterogeneous Uptake and Oxidation of Sulfur Dioxide on Mineral Dust Particles. *J. Geophys. Res.: Atmos.* **2002**, *107*, 4713.
(18) Zhang, X.; Zhuang, G.; Chen, J.; Wang, Y.; Wang, X.; An, Z.; Zhang, P. Heterogeneous Reactions of Sulfur Dioxide on Typical Mineral Particles. *J. Phys. Chem. B* **2006**, *110*, 12588−12596.
(19) Dupart, Y.; King, S. M.; Nekat, B.; Nowak, A.; Wiedensohler, A.; Herrmann, H.; David, G.; Thomas, B.; Miffre, A.; Rairoux, P.; D'Anna, B.; George, C. Mineral Dust Photochemistry Induces Nucleation Events in the Presence of SO_2. *Proc. Natl. Acad. Sci. U.S.A.* **2012**, *109*, 20842−20847.
(20) Zein, A. E.; Romanias, M. N.; Bedjanian, Y. Heterogeneous Interaction of H_2O_2 with Arizona Test Dust. *J. Phys. Chem. A* **2014**, *118*, 441−448.
(21) Yang, W.; Zhang, J.; Ma, Q.; Zhao, Y.; Liu, Y.; He, H. Heterogeneous Reaction of SO_2 on Manganese Oxides: the Effect of Crystal Structure and Relative Humidity. *Sci. Rep.* **2017**, *7*, No. 4550.
(22) Park, J. Y.; Jang, M. Heterogeneous Photooxidation of Sulfur Dioxide in the Presence of Airborne Mineral Dust Particles. *RSC Adv.* **2016**, *6*, 58617−58627.
(23) Tang, M. J.; Huang, X.; Lu, K. D.; Ge, M. F.; Li, Y. J.; Cheng, P.; Zhu, T.; Ding, A. J.; Zhang, Y. H.; Gligorovski, S.; Song, W.; Ding, X.; Bi, X. H.; Wang, X. M. Heterogeneous Reactions of Mineral Dust Aerosol: Implications for Tropospheric Oxidation Capacity. *Atmos. Chem. Phys.* **2017**, *17*, 11727−11777.
(24) Adams, J. W.; Rodriguez, D.; Cox, R. A. The uptake of SO_2 on Saharan dust: a flow tube study. *Atmos. Chem. Phys.* **2005**, *5*, 2679−2689.
(25) Li, L.; Chen, Z. M.; Zhang, Y. H.; Zhu, T.; Li, J. L.; Ding, J. Kinetics and mechanism of heterogeneous oxidation of sulfur dioxide by ozone on surface of calcium carbonate. *Atmos. Chem. Phys.* **2006**, *6*, 2453−2464.
(26) Wu, L. Y.; Tong, S. R.; Wang, W. G.; Ge, M. F. Effects of temperature on the heterogeneous oxidation of sulfur dioxide by ozone on calcium carbonate. *Atmos. Chem. Phys.* **2011**, *11*, 6593−6605.
(27) Park, J.; Jang, M.; Yu, Z. Heterogeneous Photo-oxidation of SO_2 in the Presence of Two Different Mineral Dust Particles: Gobi and Arizona Dust. *Environ. Sci. Technol.* **2017**, *51*, 9605−9613.
(28) Pozzoli, L.; Bey, I.; Rast, S.; Schultz, M.; Stier, P.; Feichter, J. Trace gas and aerosol interactions in the fully coupled model of aerosol-chemistry-climate ECHAM5-HAMMOZ: 2. Impact of heterogeneous chemistry on the global aerosol distributions. *J. Geophys. Res.: Atmos.* **2008**, *113*, No. D07309.
(29) Wang, K.; Zhang, Y.; Nenes, A.; Fountoukis, C. Implementation of dust emission and chemistry into the Community Multiscale Air Quality modeling system and initial application to an Asian dust storm episode. *Atmos. Chem. Phys.* **2012**, *12*, 10209−10237.
(30) Dong, X. Y.; Fu, J. S.; Huang, K.; Tong, D.; Zhuang, G. S. Model development of dust emission and heterogeneous chemistry within the Community Multiscale Air Quality modeling system and its application over East Asia. *Atmos. Chem. Phys.* **2016**, *16*, 8157−8180.
(31) Hoffmann, M. R.; Martin, S. T.; Choi, W. Y.; Bahnemann, D. W. Environmental Applications of Semiconductor Photocatalysis. *Chem. Rev.* **1995**, *95*, 69−96.
(32) Cwiertny, D. M.; Young, M. A.; Grassian, V. H. Chemistry and photochemistry of mineral dust aerosol. *Annu. Rev. Phys. Chem.* **2008**, *59*, 27−51.
(33) Yu, Z.; Jang, M.; Park, J. Modeling Atmospheric Mineral Aerosol Chemistry to Predict Heterogeneous Photooxidation of SO_2. *Atmos. Chem. Phys.* **2017**, *17*, 10001−10017.
(34) Yu, Z. C.; Jang, M. Simulation of Heterogeneous Photooxidation of SO_2 and NO_x in the Presence of Gobi Desert Dust Particles Under Ambient Sunlight. *Atmos. Chem. Phys.* **2018**, *18*, 14609−14622.
(35) Jang, M.; Yu, Z. Modeling Heterogeneous Oxidation of NO_x, SO_2 and Hydrocarbons in the Presence of Mineral Dust Particles under Various Atmospheric Environments. In *Multiphase Environmental Chemistry in the Atmosphere*; American Chemical Society, 2018; Vol. *1299*, pp 301−326.
(36) Environ, R. *User's Guide Comprehensive Air Quality Model with Extensions*, version 6.50; ENVIRON Intl. Corp Novato: Calif, 2019.
(37) Liang, J. Y.; Jacobson, M. Z. A study of sulfur dioxide oxidation pathways over a range of liquid water contents, pH values, and temperatures. *J. Geophys. Res.: Atmos.* **1999**, *104*, 13749−13769.
(38) Huang, L.; Zhao, Y.; Li, H.; Chen, Z. Kinetics of Heterogeneous Reaction of Sulfur Dioxide on Authentic Mineral Dust: Effects of Relative Humidity and Hydrogen Peroxide. *Environ. Sci. Technol.* **2015**, *49*, 10797−10805.
(39) Dupart, Y.; Fine, L.; D'Anna, B.; George, C. Heterogeneous Uptake of NO_2 on Arizona Test Dust under UV-A Irradiation: An Aerosol Flow Tube Study. *Aeolian Res.* **2014**, *15*, 45−51.
(40) Chang, J.; Brost, R.; Isaksen, I.; Madronich, S.; Middleton, P.; Stockwell, W.; Walcek, C. A three-dimensional Eulerian acid deposition model: Physical concepts and formulation. *J. Geophys. Res.: Atmos.* **1987**, *92*, 14681−14700.
(41) Carter, W. P. Development of the SAPRC-07 chemical mechanism. *Atmos. Environ.* **2010**, *44*, 5324−5335.
(42) Hutzell, W.; Luecken, D.; Appel, K.; Carter, W. Interpreting predictions from the SAPRC07 mechanism based on regional and continental simulations. *Atmos. Environ.* **2012**, *46*, 417−429.
(43) Nenes, A.; Pandis, S. N.; Pilinis, C. ISORROPIA: A New Thermodynamic Equilibrium Model for Multiphase Multicomponent Inorganic Aerosols. *Aquat. Geochem.* **1998**, *4*, 123−152.
(44) Astitha, M.; Lelieveld, J.; Kader, M. A.; Pozzer, A.; De Meij, A. Parameterization of dust emissions in the global atmospheric chemistry-climate model EMAC: impact of nudging and soil properties. *Atmos. Chem. Phys.* **2012**, *12*, 11057.
(45) Klingmüller, K.; Metzger, S.; Abdelkader, M.; Karydis, V.; Stenchikov, G. L.; Pozzer, A.; Lelieveld, J. Revised mineral dust emissions in the atmospheric chemistry-climate model EMAC (based on MESSy 2.52). *Geoscience* **2017**, *11*, 989−1008.
(46) Sun, J.; Zhang, M.; Liu, T. Spatial and temporal characteristics of dust storms in China and its surrounding regions, 1960−1999: Relations to source area and climate. *J. Geophys. Res.: Atmos.* **2001**, *106*, 10325−10333.
(47) Ke-Yi, C. The Northern Path of Asian Dust Transport from the Gobi Desert to North America. *Atmos. Ocean. Sci. Lett.* **2010**, *3*, 155−159.
(48) Yu, Y.; Kalashnikova, O. V.; Garay, M. J.; Notaro, M. Climatology of Asian dust activation and transport potential based on MISR satellite observations and trajectory analysis. *Atmos. Chem. Phys.* **2019**, *19*, 363−378.
(49) Kim, D.; Chin, M.; Yu, H. B.; Pan, X. H.; Bian, H. S.; Tan, Q.; Kahn, R. A.; Tsigaridis, K.; Bauer, S. E.; Takemura, T.; Pozzoli, L.; Bellouin, N.; Schulz, M. Asian and Trans-Pacific Dust: A Multimodel and Multiremote Sensing Observation Analysis. *J. Geophys. Res.: Atmos.* **2019**, *124*, 13534−13559.
(50) Stein, A.; Draxler, R. R.; Rolph, G. D.; Stunder, B. J.; Cohen, M.; Ngan, F. NOAA's HYSPLIT atmospheric transport and dispersion modeling system. *Bull. Am. Meteorol. Soc.* **2015**, *96*, 2059−2077.
(51) Scheuvens, D.; Kandler, K. On Composition, Morphology, and Size Distribution of Airborne Mineral Dust. In *Mineral Dust: A Key Player in the Earth System*; Knippertz, P.; Stuut, J.-B. W., Eds.; Springer: Netherlands: Dordrecht, 2014; pp 15−49.

https://dx.doi.org/10.1021/acsearthspacechem.0c00074
ACS Earth Space Chem. XXXX, XXX, XXX−XXX

(52) Kim, H.; Zhang, Q.; Heo, J. Influence of intense secondary aerosol formation and long-range transport on aerosol chemistry and properties in the Seoul Metropolitan Area during spring time: results from KORUS-AQ. *Atmos. Chem. Phys.* **2018**, *18*, 7149−7168.
(53) Lee, S.; Kim, J.; Choi, M.; Hong, J.; Lim, H.; Eck, T. F.; Holben, B. N.; Ahn, J.-Y.; Kim, J.; Koo, J.-H. Analysis of long-range transboundary transport (LRTT) effect on Korean aerosol pollution during the KORUS-AQ campaign. *Atmos. Environ.* **2019**, *204*, 53−67.
(54) Kong, L. D.; Zhao, X.; Sun, Z. Y.; Yang, Y. W.; Fu, H. B.; Zhang, S. C.; Cheng, T. T.; Yang, X.; Wang, L.; Chen, J. M. The effects of nitrate on the heterogeneous uptake of sulfur dioxide on hematite. *Atmos. Chem. Phys.* **2014**, *14*, 9451−9467.
(55) Ma, Q. X.; He, H. Synergistic effect in the humidifying process of atmospheric relevant calcium nitrate, calcite and oxalic acid mixtures. *Atmos. Environ.* **2012**, *50*, 97−102.
(56) Tang, M. J.; Cziczo, D. J.; Grassian, V. H. Interactions of Water with Mineral Dust Aerosol: Water Adsorption, Hygroscopicity, Cloud Condensation, and Ice Nucleation. *Chem. Rev.* **2016**, *116*, 4205−4259.
(57) Guo, H.; Sullivan, A. P.; Campuzano-Jost, P.; Schroder, J. C.; Lopez-Hilfiker, F. D.; Dibb, J. E.; Jimenez, J. L.; Thornton, J. A.; Brown, S. S.; Nenes, A.; Weber, R. J. Fine particle pH and the partitioning of nitric acid during winter in the northeastern United States. *J. Geophys. Res.: Atmos.* **2016**, *121*, 10355−10376.
(58) Wang, Q.; Dong, X.; Fu, J. S.; Xu, J.; Deng, C.; Jiang, Y.; Fu, Q.; Lin, Y.; Huang, K.; Zhuang, G. Environmentally dependent dust chemistry of a super Asian dust storm in March 2010: observation and simulation. *Atmos. Chem. Phys.* **2018**, *18*, 3505−3521.
(59) Levin, Z.; Teller, A.; Ganor, E.; Yin, Y. On the interactions of mineral dust, sea-salt particles, and clouds: A measurement and modeling study from the Mediterranean Israeli Dust Experiment campaign. *J. Geophys. Res.: Atmos.* **2005**, *110*, No. D20202.
(60) Barahona, D.; West, R. E. L.; Stier, P.; Romakkaniemi, S.; Kokkola, H.; Nenes, A. Comprehensively accounting for the effect of giant CCN in cloud activation parameterizations. *Atmos. Chem. Phys.* **2010**, *10*, 2467−2473.
(61) Kalkavouras, P.; Bossioli, E.; Bezantakos, S.; Bougiatioti, A.; Kalivitis, N.; Stavroulas, I.; Kouvarakis, G.; Protonotariou, A. P.; Dandou, A.; Biskos, G. New particle formation in the southern Aegean Sea during the Etesians: importance for CCN production and cloud droplet number. *Atmos. Chem. Phys.* **2017**, *17*, 172−192.
(62) Aas, W.; Mortier, A.; Bowersox, V.; Cherian, R.; Faluvegi, G.; Fagerli, H.; Hand, J.; Klimont, Z.; Galy-Lacaux, C.; Lehmann, C. M. Global and regional trends of atmospheric sulfur. *Sci. Rep.* **2019**, *9*, No. 953.
(63) Zheng, B.; Tong, D.; Li, M.; Liu, F.; Hong, C.; Geng, G.; Li, H.; Li, X.; Peng, L.; Qi, J. Trends in China's anthropogenic emissions since 2010 as the consequence of clean air actions. *Atmos. Chem. Phys.* **2018**, *18*, 14095−14111.
(64) Ponczek, M.; George, C. Kinetics and Product Formation during the Photooxidation of Butanol on Atmospheric Mineral Dust. *Environ. Sci. Technol.* **2018**, *52*, 5191−5198.
(65) Zeineddine, M. N.; Romanias, M. N.; Gaudion, V.; Riffault, V.; Thevenet, F. Heterogeneous Interaction of Isoprene with Natural Gobi Dust. *ACS Earth Space Chem.* **2017**, *1*, 236−243.
(66) Yu, Z. C.; Jang, M. Atmospheric Processes of Aromatic Hydrocarbons in the Presence of Mineral Dust Particles in an Urban Environment. *ACS Earth Space Chem.* **2019**, *3*, 2404−2414.
(67) Schmidt, M.; Jansen van Beek, S. M.; Abou-Ghanem, M.; Oliynyk, A. O.; Locock, A. J.; Styler, S. A. Production of Atmospheric Organosulfates via Mineral-Mediated Photochemistry. *ACS Earth Space Chem.* **2019**, *3*, 424−431.

https://dx.doi.org/10.1021/acsearthspacechem.0c00074
ACS Earth Space Chem. XXXX, XXX, XXX−XXX